Electronic Supplementary Material (ESI) for Nanoscale.

Electronic Supplementary Information (ESI)

Solvent Manipulation of the Pre-reduction Metal-Ligand Complex and Particle-Ligand Binding for Controlled Synthesis of Pd Nanoparticles

Wenhui Li,[a] Michael G. Taylor,[b] Dylan Bayerl,[b] Saeed Mozaffari,[a] Mudit Dixit,[b] Sergei Ivanov,[c] Soenke Seifert,[d] Byeongdu Lee,[e] Narasimhamurthy Shanaiah,[a] Yubing Lu,[a] Libor Kovarik,[f] Giannis Mpourmpakis,[b,]* and Ayman M. Karim[a,]*

[a] Department of Chemical Engineering, Virginia Polytechnic Institute and State University, Blacksburg, VA 24060, United States

[b] Department of Chemical Engineering, University of Pittsburgh, Pittsburgh, PA 15261

[c] Center for Integrated Nanotechnologies, Los Alamos National Laboratory, Los Alamos, NM 87545, United States

[d] Advanced Photon Source, Argonne National Laboratory, Argonne, IL 60439, United States

[e] X-ray Science Division, Argonne National Laboratory, Argonne, IL 60439, United States

[f] Institute for Integrated Catalysis, and Physical and Computational Science Directorate, Pacific Northwest National Laboratory, P.O. Box 999, Richland, Washington 99352, United States

* Corresponding authors: gmpourmp@pitt.edu, amkarim@vt.edu

Estimations of number of nanoparticles and extent of reaction (reacted Pd atoms in nanoparticles)

The estimations of number of nanoparticles and extent of reaction follow the same methodology with our previous study[1]. First, I(0) can be obtained by extrapolation of I(q) for q → 0. $\langle {V_p}^2 \rangle$ is the average square of nanoparticle volume, which can be calculated with the following equation:

$$\langle {V_p}^2 \rangle = \left(\frac{4\pi}{3}\right)^2 \int_0^\infty f(r) r^6 \, dr \qquad (S1)$$

where $f(r)$ is the Schulz-Zimm distribution function shown in Equation (5) in the main text:

$$f(r) = \frac{r^z}{\Gamma(z+1)} \left[\frac{z+1}{r_{avg}}\right]^{z+1} exp\, exp \left(-\frac{(z+1)r}{r_{avg}}\right) \qquad (S2)$$

where $z = (\frac{r_{avg}}{\sigma)}^2 - 1$. r_{avg} is the average radius of nanoparticles; σ is the standard deviation (both obtained from the SAXS fit) and Γ is the gamma function.

Thus, the number of nanoparticles can be calculated based on Eqn. S(3):

$$N_p = \frac{I(0)}{(\Delta\rho)^2 \langle {V_p}^2 \rangle} = \frac{I(0)}{(\Delta\rho)^2 \left(\frac{4\pi}{3}\right)^2 \int_0^\infty f(r) r^6 \, dr} \qquad (S3)$$

The total reacted Pd concentration (i.e. Pd concentration in nanoparticles A) can be calculated using the number of atoms in each nanoparticle, N and the Shulz-Zimm distribution as shown in equations S(4-5):

$$N = \frac{\pi 4 r^3 \rho N_A}{3 M_w} \qquad (S4)$$

Where r is the radius of the nanoparticle, ρ is the nanoparticle density, and M_w is the molecular weight and for Pd nanoparticles, ρ is taken as bulk Pd density, 12.02 g / cm^3, and M_w = 106.4 g / mol.

The reacted Pd concentration in nanoparticles A can be calculated as:

$$A = \frac{N_p}{N_A} \int_0^\infty f(r) N \, dr \qquad (S5)$$

Finally, the extent of reaction $\eta = \frac{A}{C_0}$, where C_0 is the total Pd concentration (10 mM).

Extracting the rates of nucleation and growth from experimental data

The nucleation and growth are temporally overlapped as shown in Figure S8 but these two processes contribute to different observables in the in-situ SAXS. Namely, the nucleation contributes to the increase in number of nanoparticles, while both the nucleation and growth contribute to the increase in diameter and consequently the total scattering intensity (total metal in nanoparticles). Therefore, as we showed previously[4], the nucleation rate can be extracted from the plot of number of nanoparticles versus time by calculating the slope. Similarly, the slope of total number of atoms in all formed nanoparticles represents the sum of nucleation and growth rates. Below are the details of these calculations:

Nucleation rate shown in Eqn. (1) is the number of nuclei per unit reaction volume per unit time (number of nuclei L^{-1} s^{-1}). Therefore, the nucleation rate from the experiments at a short time interval (Δt) can be estimated as follows[1]:

$$\text{Nucleation Rate} = \frac{\Delta N_P}{\Delta t} \tag{S6}$$

To make a comparison between the rates of growth and nucleation during synthesis of Pd nanoparticles, it is necessary that both rates use the same units (i.e. M s^{-1}). Thus, in Eqn. (S5), we accounted for the nucleus size (n, the number of atoms per nucleus) and Avogadro's number (N_A) to make the units the same (M s^{-1})[1]. The smallest nanoparticle size measured via SAXS in different solvents was similar and ranged from ~0.6-0.8 nm (~4-13 atoms/nucleus (ref[5])). In the absence of any further information on the size of nucleus, we considered Pd nucleus in different solvents to consist of 4 atoms (n=4). The reported values of atoms/nucleus for different metallic nanoparticles (including Pd, Pt, Ir, and Au) ranged from 4-10[1, 6-10], and it is consistent with our estimated value of nucleus size. Additionally, the trend shown in Figure 1 was not affected considering nucleus size in the range of 0.6-0.8 nm.

After obtaining the rate of nucleation, the growth rate can be extracted from the slope of total concentration of atoms in all formed nanoparticles (A). "A" quantifies both the formation of nanoparticles (nucleus) and nanoparticle growth.

Therefore, the growth rate can be written as:

$$\text{Growth Rate} = \frac{\Delta A}{\Delta t} - \left(\frac{\Delta N_P}{\Delta t} \times \frac{n}{N_A}\right) \tag{S7}$$

In addition, the dimensionless Growth/Nucleation rate can be obtained as follows[1]:

$$\left(\frac{\text{Growth Rate}}{\text{Nucleation Rate}}\right) = \frac{\frac{\Delta A}{\Delta t} - \left(\frac{\Delta N_P}{\Delta t} \times \frac{n}{N_A}\right)}{\left(\frac{\Delta N_P}{\Delta t} \times \frac{n}{N_A}\right)} = \frac{\frac{\Delta A}{\Delta t}}{\left(\frac{\Delta N_P}{\Delta t} \times \frac{n}{N_A}\right)} - 1 \tag{S8}$$

We note that the choice of *n* (atoms/nucleus) would make a difference in extracting the growth rate **only** in toluene where the nucleation rate was the highest. In all other solvents, the nucleation rate (in M.s^{-1}) is much lower than that of growth, even if *n* =10-20 instead of 4 atoms/nucleus. However, the choice of *n* does not affect the trend between the different solvents.

Damköhler number (*Da*) identifying kinetic control reaction

$Da \approx r^2 (\frac{k_{3-growth}[A]}{D_{ab}})$ was used as a criterion of identifying if the nucleation and growth are diffusion controlled or kinetically controlled reactions, where [*A*] is the metal concentration, $k_{3-growth}$ is the surface growth rate constant, and *r* is the radius of the nanoparticle[2]. D_{ab} is the diffusion coefficient of metal complex in the solvents, and it can be estimated based on Stokes-Einstein equation[3]; $D_{ab} = \frac{k_B T}{6\pi R_e \mu}$. Here T, k_B, R_e and µ represent the absolute temperature, the Boltzmann constant, the effective radius of the diffusing species (ligated metal complex in our reaction system), and the solvent viscosity, respectively. The value of *Da* for the nanoparticles with the size of 2 nm was estimated to be in the range of 10^{-8}-10^{-9}. This further confirms that the growth is kinetic reaction controlled rather than diffusion controlled.

Precursor speciation calculations from density functional theory (DFT)

For the speciation calculations seen in Table S4, the Gibbs free energy of reaction was used to calculate the relative concentrations of each type of precursor (before reduction). As the solvent bindings are highly exothermic for the coordinating solvents and the solvents are coordinated in high amounts of excess, the assumption was made that all of the TOP will be reacting directly with the $Pd(OAc)_2(solv)_2$ precursors. This assumption allows the concentration of the different precursors to be modelled as the equilibrium of the following reactions:

$$Pd(OAc)_2(solv)_2 + TOP \leftrightarrow solv + Pd(OAc)_2(TOP)(solv) \tag{S9}$$

and

$$Pd(OAc)_2(TOP)(solv) + TOP \leftrightarrow solv + Pd(OAc)_2(TOP)_2 \tag{S10}$$

From the DFT free energy calculations, the ΔG_{Rxns} of Eqn. S9/S10 can be found in Figure 3.

From here, the equilibrium of the reaction in Eqn. S9 can be expressed as:

$$K_{eq,S9} = exp\left(-\frac{\Delta G_{Rxn,S9}}{RT}\right) = \frac{[Pd(OAc)_2(TOP)(Solv)]*[Solv]}{[TOP][Pd(OAc)_2(Solv)_2]} \tag{S11}$$

While Eqn. S10 can be expressed as:

$$K_{eq,S10} = exp\left(-\frac{\Delta G_{Rxn,S10}}{RT}\right) = \frac{[Pd(OAc)_2(TOP)_2]*[Solv]}{[TOP][Pd(OAc)_2(Solv)(TOP)]} \tag{S12}$$

Where [y] represents the concentration (molarity) of species y, R is the gas constant, and T is the temperature (298.15 K). Because all of the $Pd(OAc)_2$ is conserved up to the addition of the TOP and there are no TOP-containing compounds initially, we set:

$$[Pd(OAc)_2(solv)_2]^0 = [Pd(OAc)_2]^{Init}\ ,\ [Pd(OAc)_2(TOP)_2]^0 = [Pd(OAc)_2(solv)(TOP)]^0 = 0 \tag{S13}$$

and

$$[TOP]^0 = [TOP]^{Added} \text{ and } [solv]^0 = \rho_{solv}/MW_{solv} \tag{S14}$$

Where $[X]^0$ represents the initial concentration of X before the TOP reactions occur, ρ_{solv} and MW_{solv} represent the density and molecular weight of the solvents, respectively, $[Pd(OAc)_2]^{Init}$ represents the concentration of $Pd(OAc)_2$ initially added to the solvent, and $[TOP]^{Added}$ represents the concentration of TOP added to the solvent/Pd solution. Using these initial values and the combination of Eqns. S11 –S12 (substituting extents of reaction) there become 2 equations and 2 unknowns:

$$exp\left(-\frac{\Delta G_{Rxn,S9}}{RT}\right) = \frac{(\varepsilon_{S9}-\varepsilon_{S10})*([solv]^0+\varepsilon_{S9}+\varepsilon_{S10})}{([TOP]^{Added}-\varepsilon_{S9}-\varepsilon_{S10})*([Pd(OAc)_2]^{Init}-\varepsilon_{S9})} \tag{S15}$$

and,

$$exp\left(-\frac{\Delta G_{Rxn,S10}}{RT}\right) = \frac{(\varepsilon_{S10})*([Solv]^0+\varepsilon_{S9}+\varepsilon_{S10})}{([TOP]^{Added}-\varepsilon_{S9}-\varepsilon_{S10})*(\varepsilon_{S9}-\varepsilon_{S10})} \tag{S16}$$

Where, ε_{s9} and ε_{s10}, represent the extents of reaction of reactions S9 and S10, respectively. Thus, the relative concentrations of each of the precursors (speciation) are solvable.

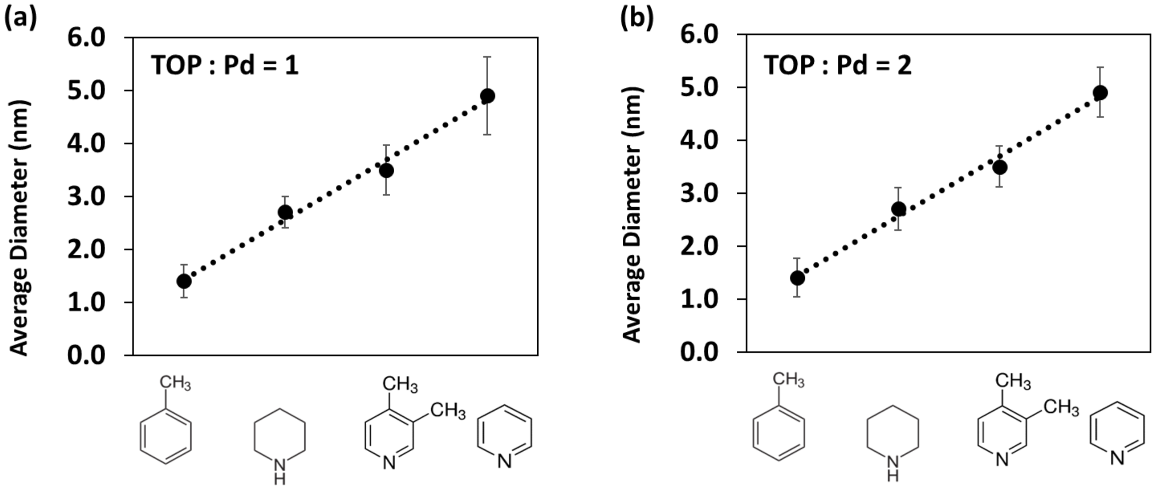

Figure S1 Effect of solvent on final Pd nanoparticle size. (a) TOP : Pd =1; (b) TOP : Pd = 2. The synthesis procedures are the same as described in experimental section. Pd(OAc)$_2$ = 10 mM, solv : hexanol = 50 : 50, T = 100 °C. The sizes were taken when no more increase was observed by SAXS measurements. The dotted lines show the observed size trend but do not represent a theoretical or empirical fit.

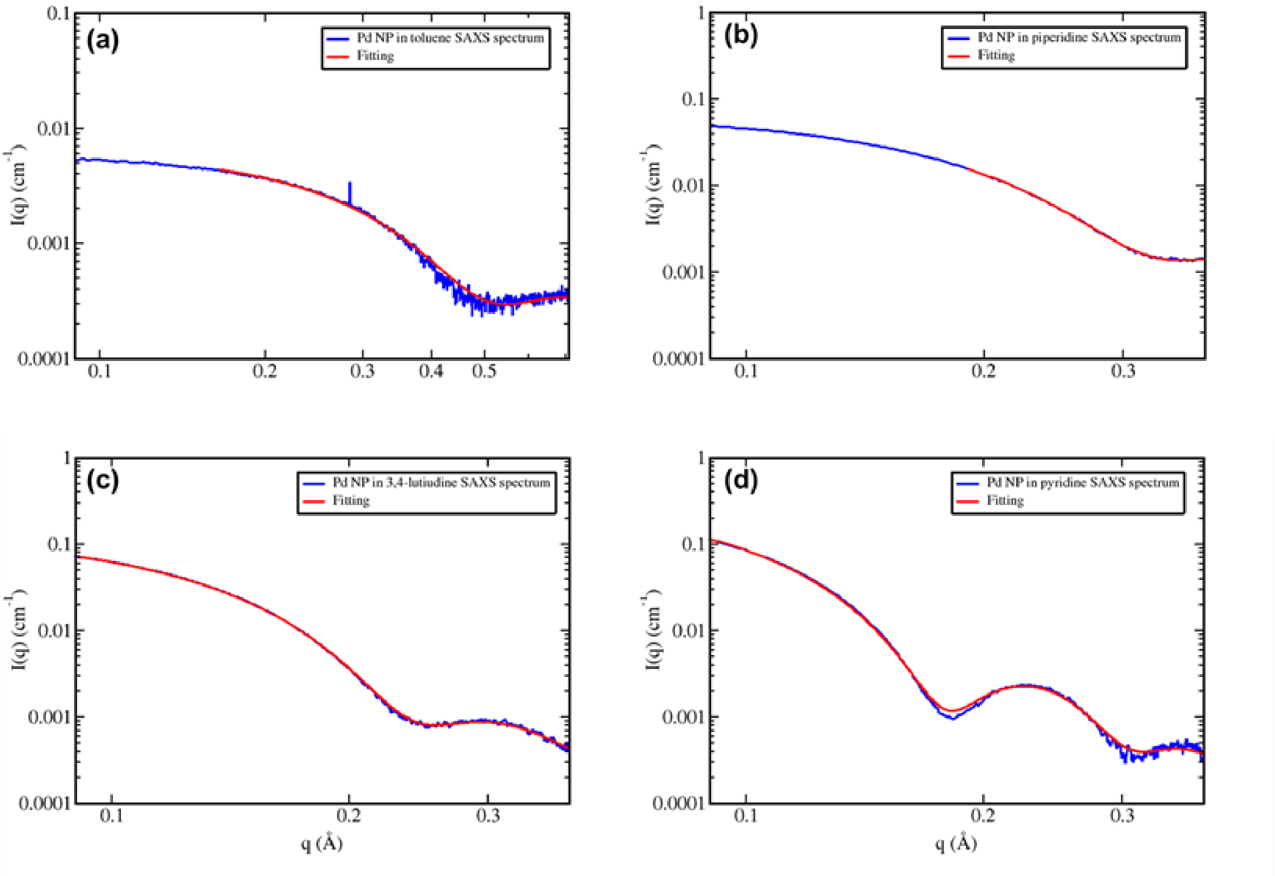

Figure S2 Representative in-situ SAXS spectra of the nanoparticles in the original solution at the end of the synthesis (when the size and nanoparticle concentration stopped increasing) and fitting curves synthesized in different solvents: **(a)** toluene, 1.4 nm ± 0.4 nm **(b)** piperidine, 2.7 nm ± 0.3 nm **(c)** 3,4-lutidine, 3.5 ± 0.5 nm **(d)** pyridine, 4.8 nm ± 0.6 nm at TOP : Pd = 1, $Pd(OAc)_2$ concentration = 10 mM, solvent : hexanol = 1:1, T = 100℃.

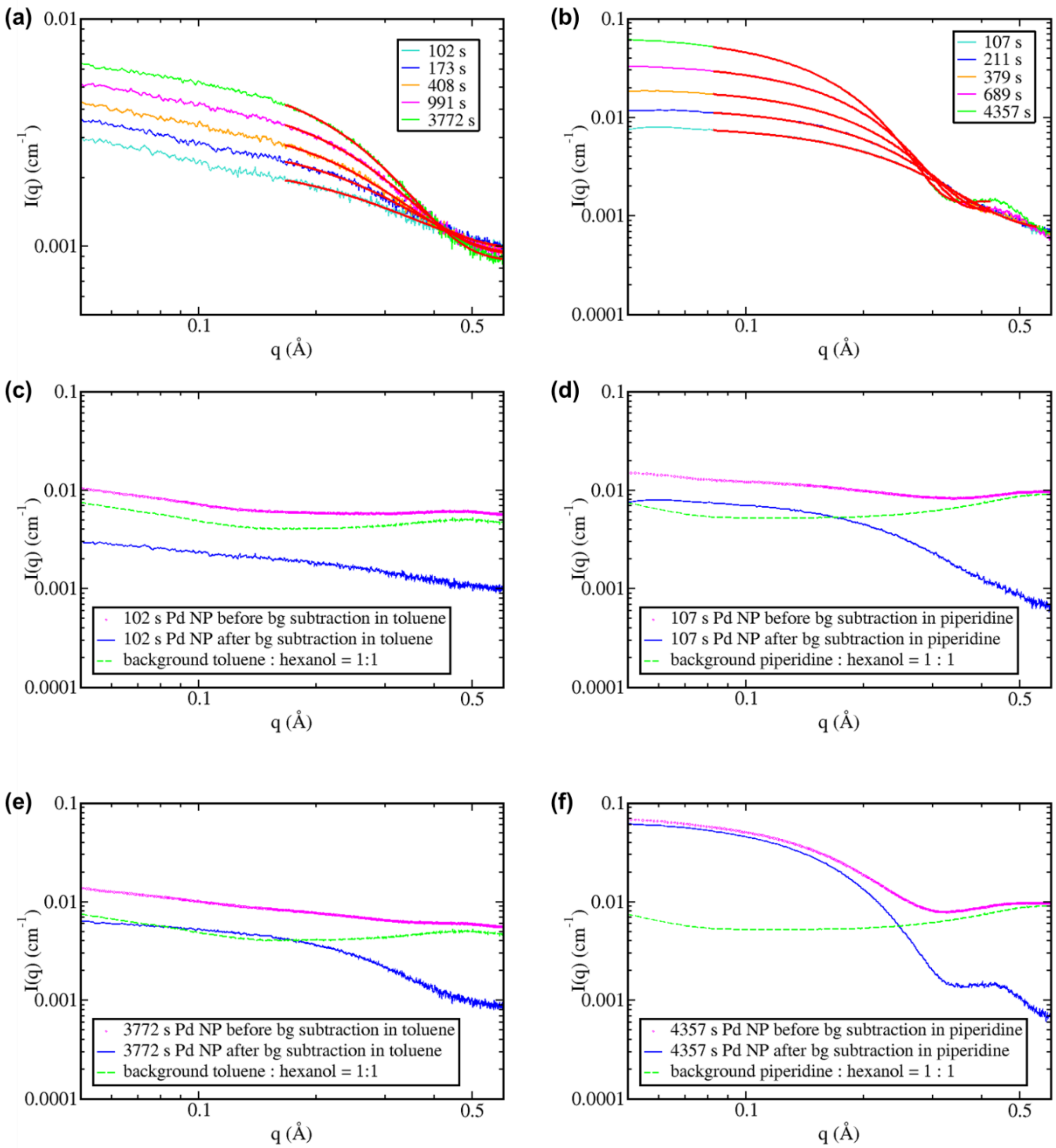

Figure S3 Representative in-situ SAXS curves in toluene and piperidine with smallest final nanoparticle size among the four solvents at TOP : Pd = 1: **(a)** and **(b)** SAXS curves after background subtraction and fitting curves (in red) at different times in toluene and piperidine. **(c)**, **(d)**, **(e)** and **(f)** are original SAXS curves, SAXS curves after background subtraction, and background solvent curves at early and late time of the reaction. **(c)** 102 s in toluene : hexanol = 1:1; **(d)** 107 s in piperidine : hexanol = 1:1; **(e)** 3772 s in toluene : hexanol = 1:1; **(f)** 4357 s in piperidine : hexanol = 1:1. The low amount of TOP in the solvents (4.5 µL / mL) does not affect the solvent background.

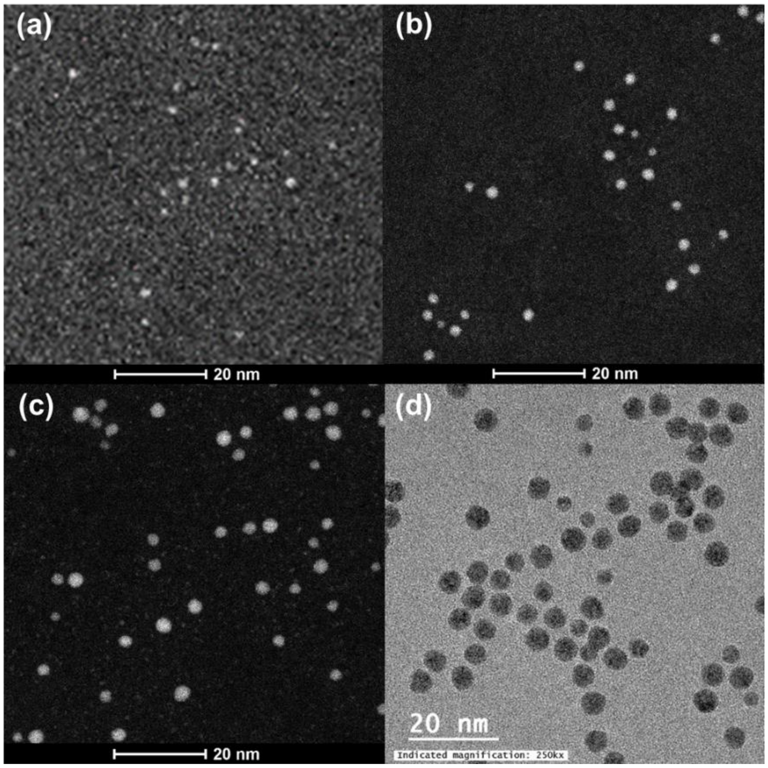

Figure S4 TEM images of Pd nanoparticles synthesized in different solvents **(a)** toluene, 1.8 nm ± 0.4 nm **(b)** piperidine, 2.6 nm ± 0.3 nm **(c)** 3,4-lutidine, 3.3 nm ± 0.4 nm **(d)** pyridine, 4.9 nm ± 0.6 nm at TOP : Pd = 1, $Pd(OAc)_2$ concentration = 10 mM, solvent : hexanol = 1:1, T = 100℃.

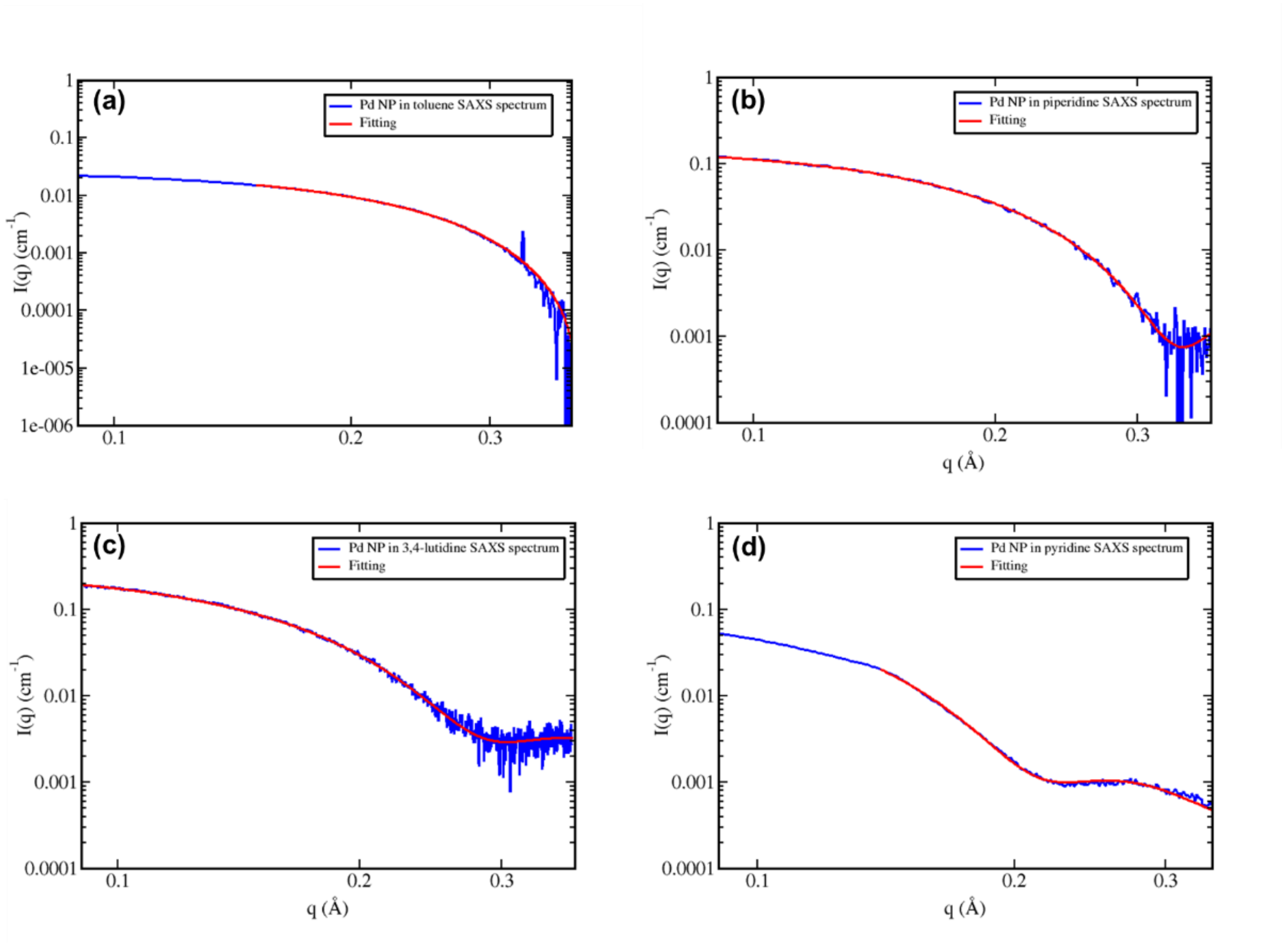

Figure S5 Representative SAXS spectra of the nanoparticles in the original solution at the end of the synthesis (when the size and nanoparticle concentration stopped increasing) and fitting curves for Pd nanoparticles synthesized in different solvents: **(a)** toluene, 1.5 nm ± 0.4 nm **(b)** piperidine, 2.5 nm ± 0.3 nm **(c)** 3,4-lutidine, 2.9 ± 0.3 nm **(d)** pyridine, 3.9 nm ± 0.6 nm at TOP : Pd = 2, $Pd(OAc)_2$ concentration = 10 mM, solvent : hexanol = 1:1, T = 100°C. **(a)** and **(d)** are in-situ SAXS spectra collected at the synchrotron; **(c)** and **(d)** are ex-situ SAXS spectra collected using Bruker N8 Horizon.

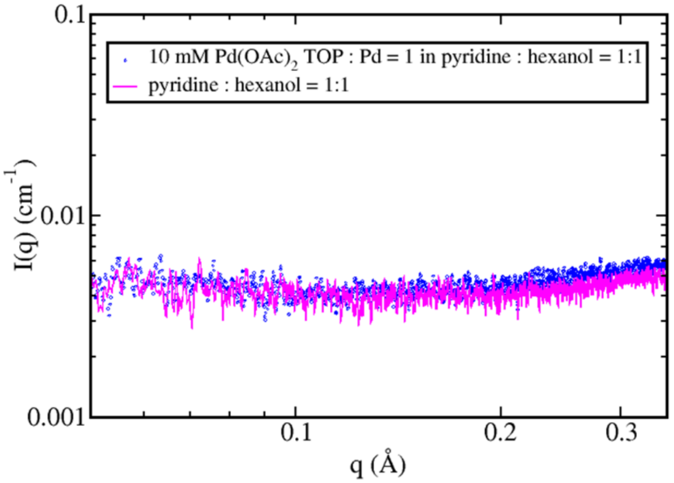

Figure S6 SAXS spectra of 10 mM Pd(OAc)$_2$ and 10 mM TOP in pyridine : hexanol = 1:1 solution (blue dots) and pyridine : hexanol = 1:1 solution (purple line)

Figure S6 shows the spectra of the pure solvent and that of the initial reaction solution before heating up overlap with each other, indicating the beam doesn't induce any reduction of the precursor. At the same time, the ex-situ synthesis, of which only the final product was measured using SAXS in Figure S7, shows similar average size and size distribution with the in-situ synthesis (two separate experiments). This result shows that the exposure to the beam does not have a significant effect on the synthesis kinetics and conclusions in this work.

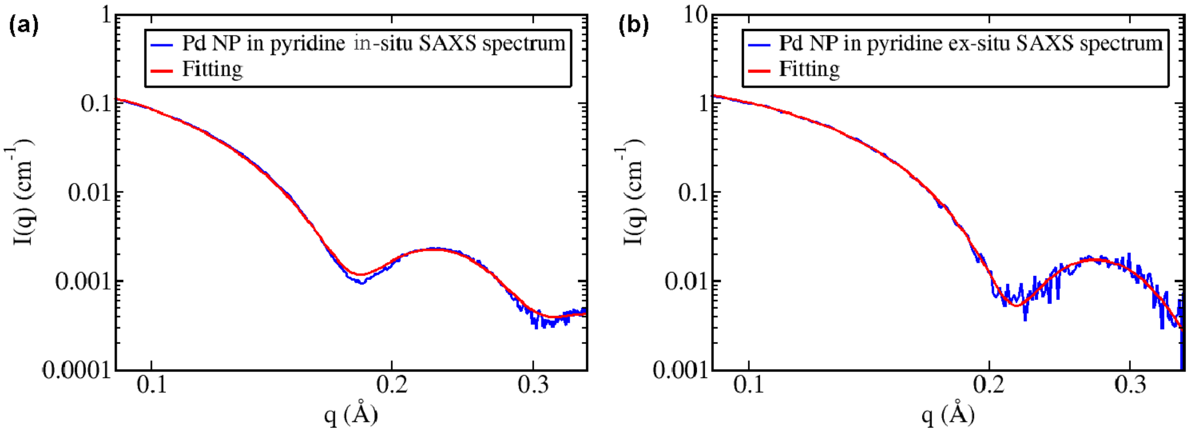

Figure S7 SAXS spectrum (blue line) and the fitting (red line) of the final product of Pd nanoparticles synthesized in pyridine and hexanol. (a) In-situ SAXS, the average diameter is 4.8 nm ± 0.6 nm. (b) Ex-situ SAXS, the average diameter is 4.4 nm ± 0.6 nm. $Pd(OAc)_2$ = 10 mM, TOP = 10 mM, pyridine : hexanol = 1:1, temperature = 100 °C, reaction time is 3 hr.

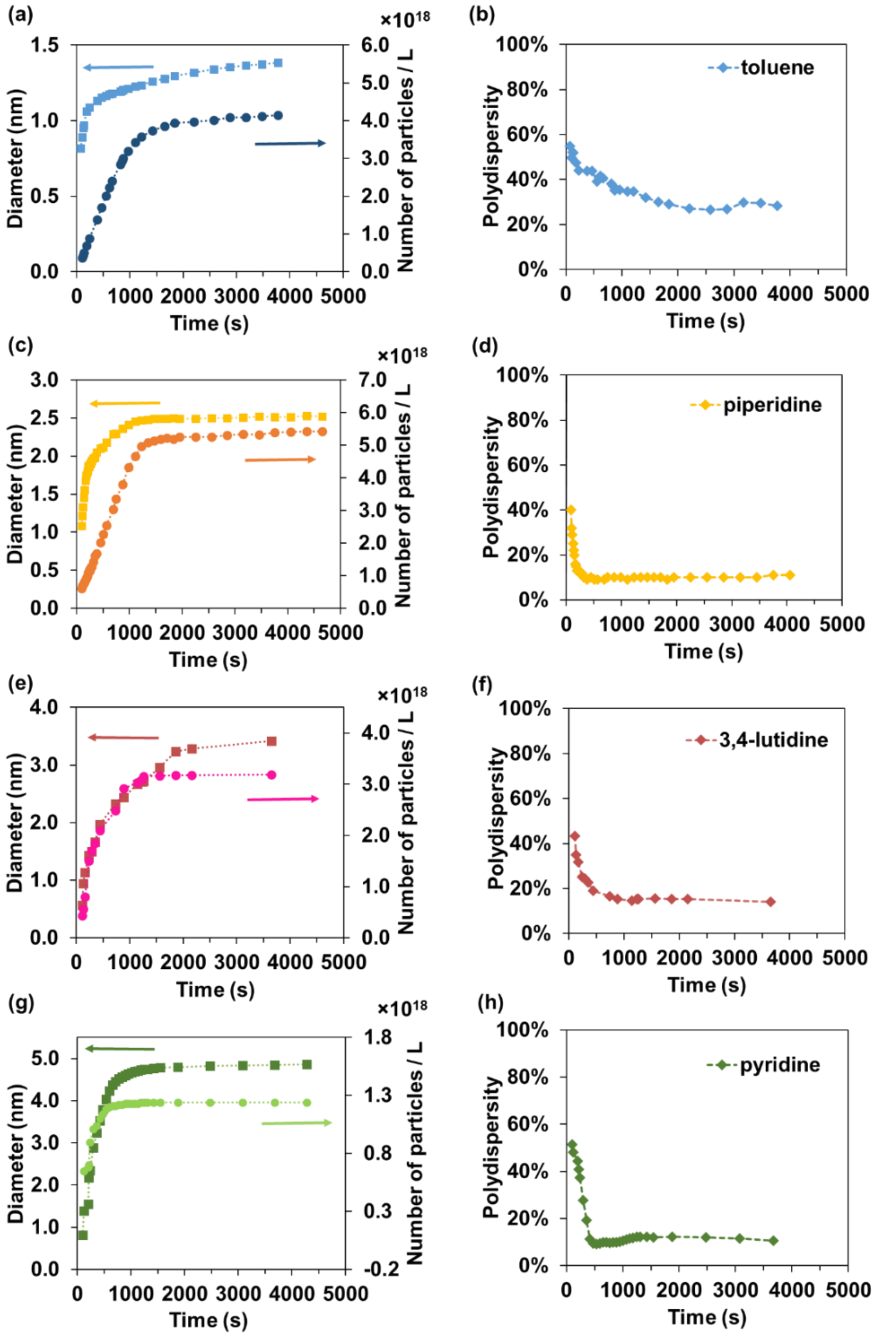

Figure S8 In-situ SAXS measurement fitting results: time evolutions of mean diameter and polydispersity in **(a)** and **(b)** toluene, **(c)** and **(d)** piperidine**,** **(e)** and **(f)** 3,4-lutidine, (g) and (h) pyridine. $Pd(OAc)_2$ concentration = 10 mM, TOP concentration = 10 mM, solvent : hexanol = 1:1, T = 100 ℃. Time 0 was defined as the time when the solution temperature reached to 100 ℃. An overlap between nucleation (increase of nanoparticle concentration) and growth (increase of nanoparticle size) was observed in all solvents, suggesting that the kinetics follow our previously proposed ligand-controlled mechanism.[4, 11, 12]

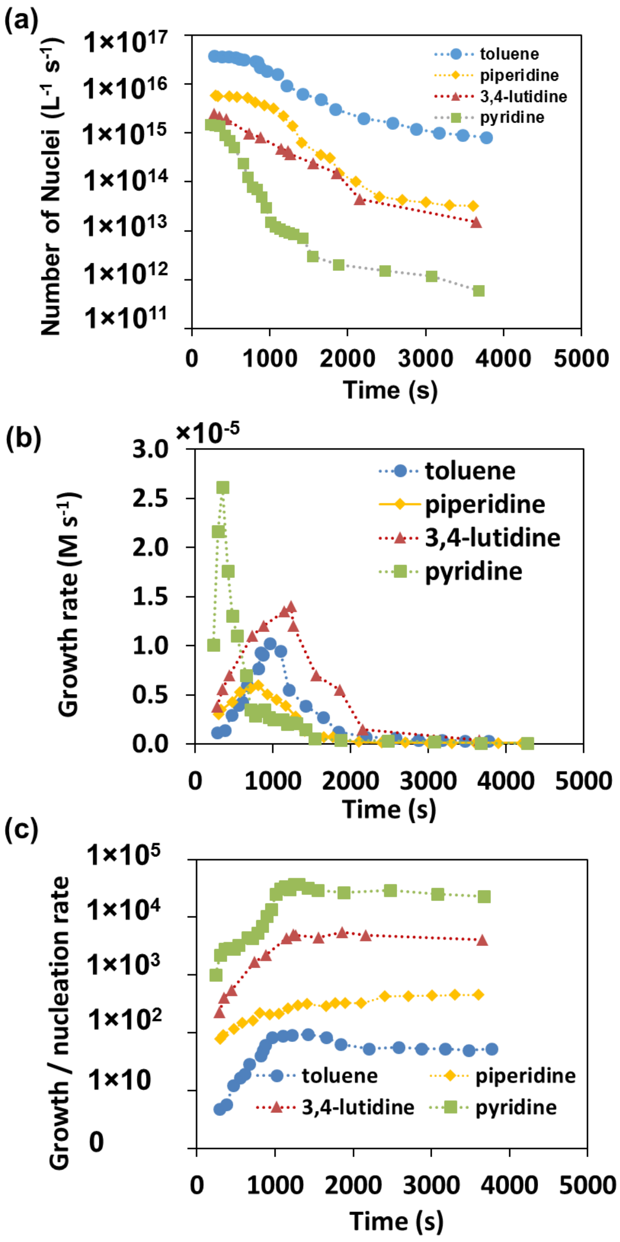

Figure S9 Kinetics extracted from in-situ SAXS in toluene, piperidine, 3,4-lutidine and pyridine during synthesis of Pd nanoparticles: Time evolution of (a) nucleation rate (i.e. number of nuclei formed per liter per second), (b) growth rate, (c) growth / nucleation rate ratio. In panel (c), the nucleation rates in (a) were multiplied by the same nucleus size (4 atoms per nucleus, see additional details in pages S-2 and S-3) and divided by Avogadro's number for all solvents in order to have the same units for nucleation and growth rates.

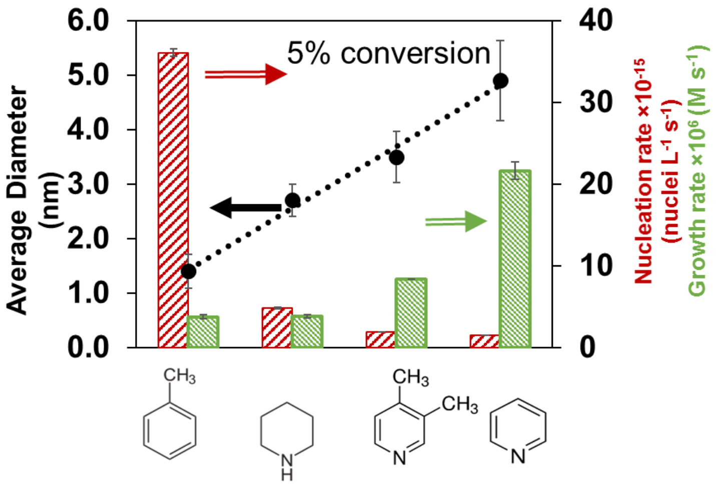

Figure S10 Final average nanoparticle size, and initial nucleation and growth rates (at 5 % Pd precursor conversion) measured in the different solvents. The error bars of the rates were calculated from the SAXS fitting error. The rates in toluene and pyridine were reproduced within 15% error from repeating in-situ experiments. The error bars represent the standard deviation of the size distribution as obtained from the fits. The dotted lines show the observed size trend but do not represent a theoretical or empirical fit. Reaction conditions: $Pd(OAc)_2$ = 10 mM, TOP : Pd = 1 (molar), solv : hexanol = 50 : 50, T = 100 °C.

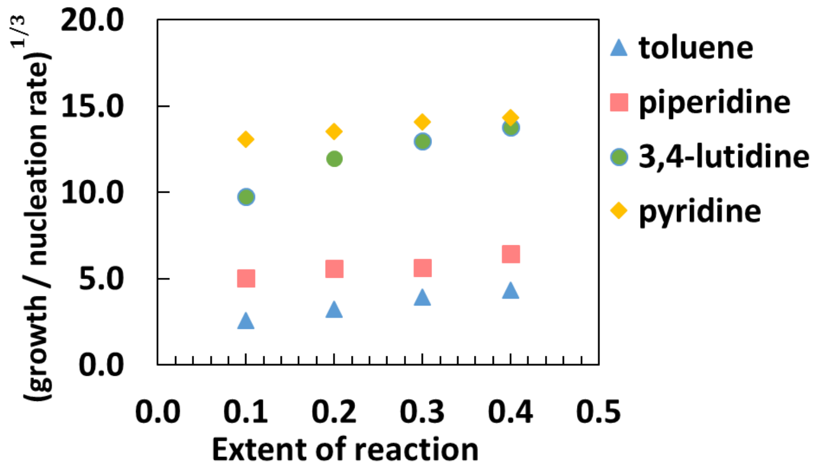

Figure S11 (Growth/nucleation rate)$^{1/3}$ as a function of extent of reaction in the different solvents. Reaction conditions: $Pd(OAc)_2$ = 10 mM, TOP : Pd = 1 (molar), solv : hexanol = 50 : 50, T = 100 °C. Detailed calculations are shown in equations S5-S7. The rate ratios (unitless) are calculated after converting both growth and nucleation rates into the same units (atom / L / s or equivalent M / s) as decribed on page S-3.

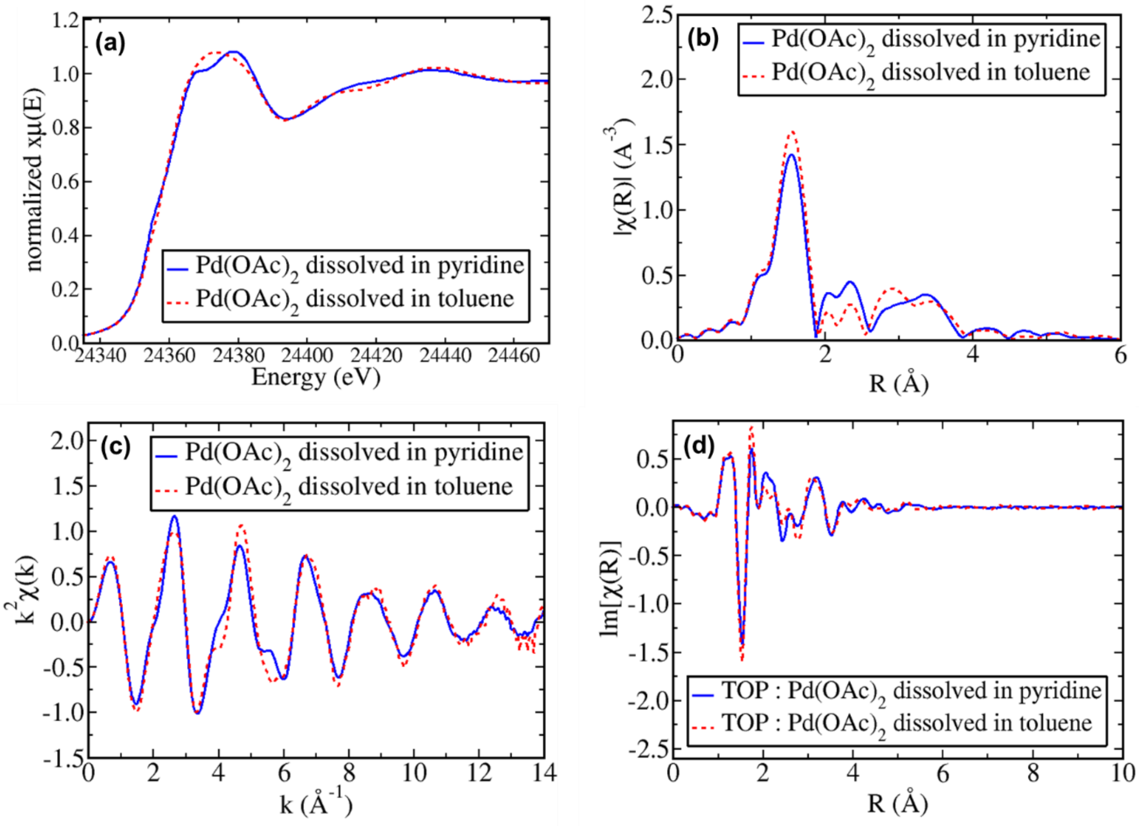

Figure S12 Pd K-edge **(a)** XANES and **(b)** EXAFS, magnitude of the Fourier transformed k^2-weighted χ(k) data (Δk= 2.5-12 Å^{-1}) and **(c)** spectra in k-space **(d)** imaginary parts for 20 mM Pd acetate in toluene and pyridine solution**.**

Table S1 EXAFS modeling results for Pd acetate (20 mM) in pyridine and toluene. The numbers in parentheses indicate the statistical error in the most significant digit obtained from the fit in Artemis (e.g. 4.3(5) = 4.3±0.5).

Pd acetate solution	$N_{PdO/N}$	$R_{PdO/N}$	σ^2_{PdO} (Å^2)	N_{PdC} trimer	R_{PdC} bridging	N_{PdO} Bridging	R_{PdO} bridging	N_{PdPd} trimer	R_{PdPd} trimer	ΔE_0	Reduced χ^2
Pyridine	4.3(5)	2.005(9)	0.003(1)	/	/	/	/	/	/	7(1)	475
Toluene	4.2(3)	2.010(6)	0.001(1)	4.8(1.9)	2.95(3)	4.8(1.8)	3.15(3)	2.2(1.4)	3.19(5)	9(2)	180

Notation: N, coordination number of absorber-backscatterer pair; R, radial absorber-backscatterer distance; σ^2, the mean square displacement of the half-path length and represents the stiffness of the bond for a single scattering path, ΔE_0, correction to the threshold energy.

(a) trans-$PdCl_2(TOP)(py)$

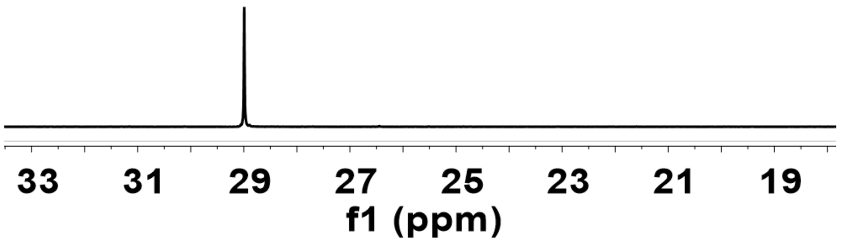

(b) trans-$PdCl_2(TOP)_2$

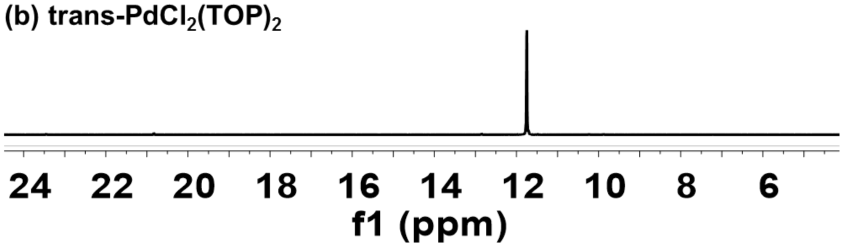

Figure S13 ^{31}P NMR of 10 mM $PdCl_2$ in pyridine with TOP ligand: **(a)** TOP : Pd = 1 with product trans-$PdCl_2(TOP)(py)$ at 29.0 ppm and **(b)** TOP : Pd = 2 with product trans-$PdCl_2(TOP)_2$ at 11.8 ppm.

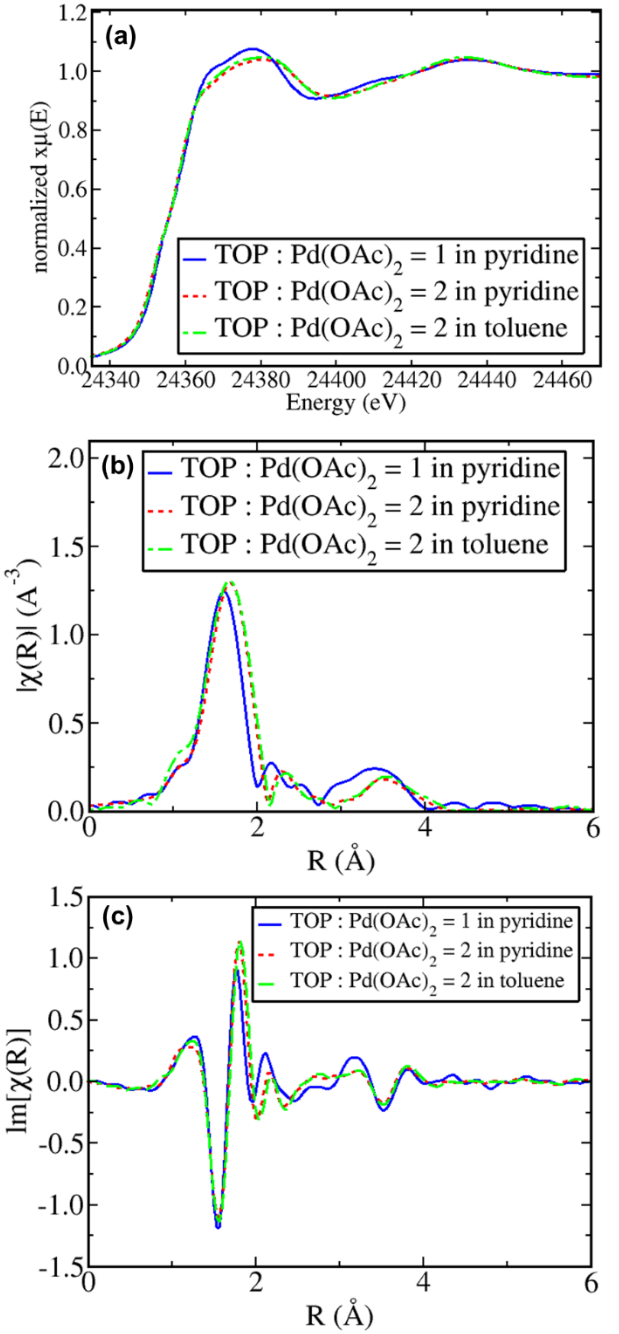

Figure S14 Pd K-edge comparison **(a)** XANES and **(b)** EXAFS magnitude and **(c)** imaginary part of the Fourier transformed k^2-weighted χ(k) data (Δk= 2.5-12 $Å^{-1}$) for TOP : $Pd(OAc)_2$ = 1 and 2, in pyridine, and TOP : $Pd(OAc)_2$ =2 in toluene. Concentration of $Pd(OAc)_2$ was 20 mM.

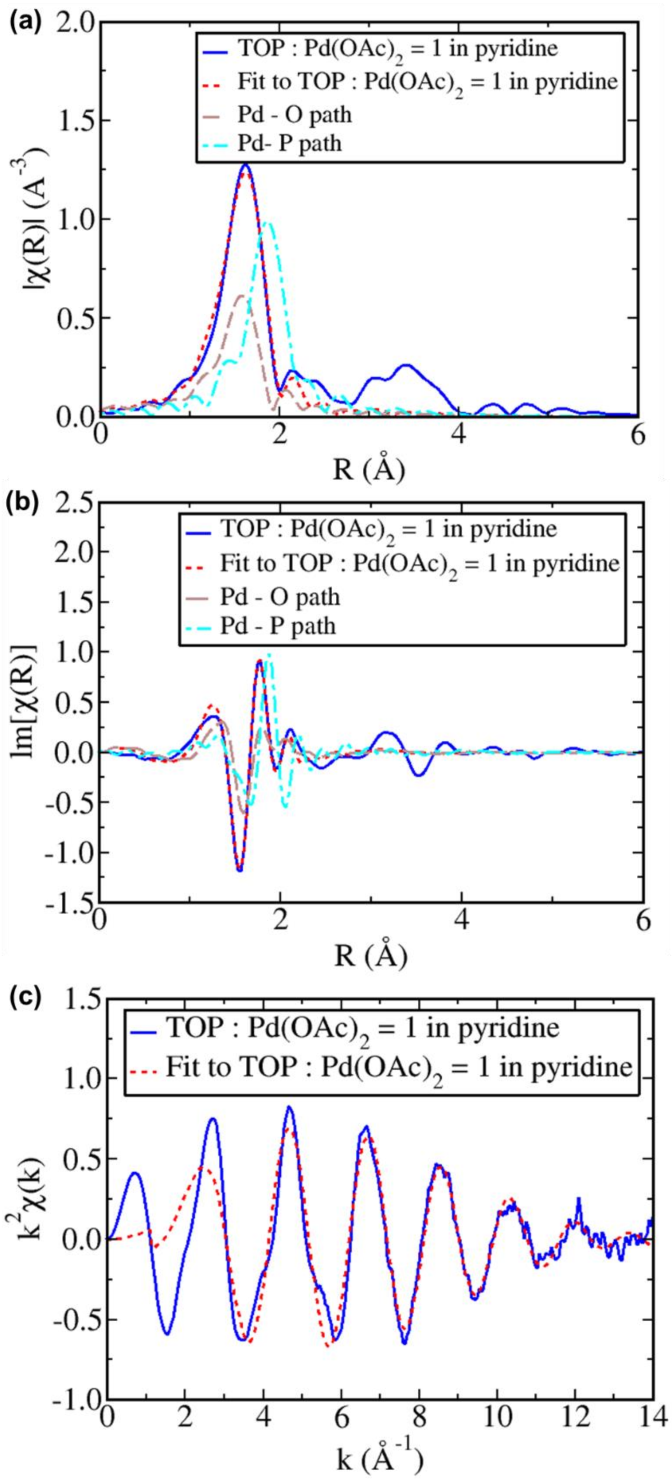

Figure S15 Pd K-edge EXAFS **(a)** magnitude and **(b)** imaginary part of the Fourier transform k^2-weighted χ(k) (Δk= 2.5-12 Å^{-1}) and the fit of 20 mM Pd acetate with 20 mM TOP in pyridine; and **(c)** fit in k-space.

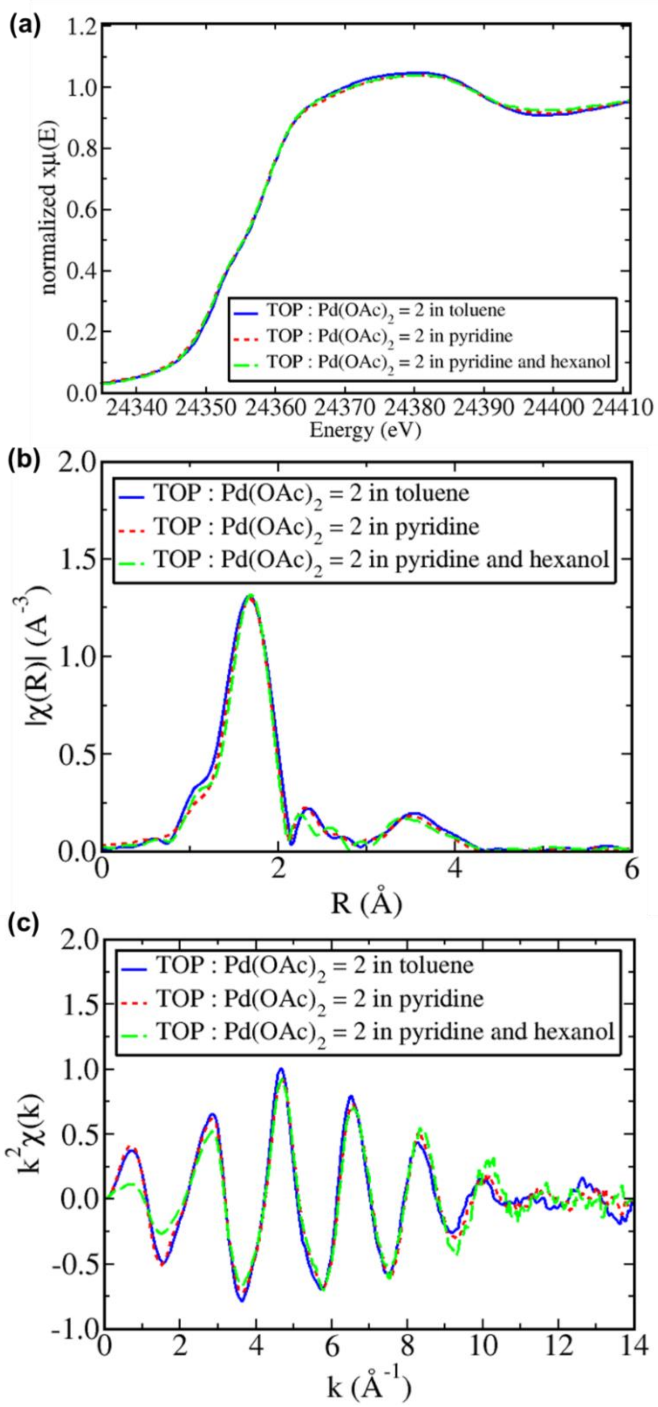

Figure S16 Pd K-edge comparison **(a)** XANES and **(b)** EXAFS, magnitude of the Fourier transformed k^2-weighted χ(k) data (Δk= 2.5-12 Å^{-1}) and **(c)** k-space of 20 mM Pd acetate with 40 mM TOP in toluene, pyridine solution, and pyridine : hexanol = 1:1 mixture. Addition of hexanol does not affect the (Pd(OAc)$_2$(TOP)$_2$) complex.

Table S2 EXAFS modeling results for Pd acetate in pyridine and toluene. The numbers in parentheses indicate the statistical error in the most significant digit obtained from the fit in Artemis (e.g. 2.6(4) = 2.6±0.4).

TOP:Pd	Solvent	N_{PdO}	$R_{PdO/N}$	σ^2_{PdO} (Å^2)	N_{PdP}	R_{PdP}	σ^2_{PdP} (Å^2)	ΔE0	Reduced χ^2
1	Pyridine	3.0(4)	2.01(1)	0.003(3)	1.0(3)	2.25(1)	0.001(1)	6(4)	110
2	Pyridine	2.6(4)	2.04(1)	0.002(2)	1.6(3)	2.32(1)	0.001(1)	11(3)	206
2	Toluene	2.8(5)	2.04(1)	0.002(2)	1.7(4)	2.34(2)	0.002(2)	11(4)	250

Notation: N, coordination number of absorber-backscatterer pair; R, radial absorber-backscatterer distance; σ^2, the mean square displacement of the half-path length and represents the stiffness of the bond for a single scattering path, ΔE_0, correction to the threshold energy.

Table S3 Mole fraction of different precursor complexes (speciation) existing in different solvents from DFT calculations at TOP : Pd = 2, T=293.15 K.

Solvent	**mol % $Pd(OAc)_2(TOP)_2$**	**mol % $Pd(OAc)_2(TOP)(Solv)$**	**mol % $Pd(OAc)_2(Solv)_2$**
Toluene	100.000	0.000	0.000
Pyridine	99.977	0.011	0.011
3,4-Lutidine	99.918	0.041	0.041
Piperidine	99.777	0.111	0.111

Table S4 Energy of displacement of acetate with hexoxy species in predominant precursors. All replacement reactions are endothermic, in contrast to solvent binding energies.

Solvent	**Hexoxy Displacement Energy (kJ/mol)**
Pyridine	24.05
Piperidine	9.53
3,4-Lutidine	35.72

Table S5 Energy of solvent displacement by hexanol in predominant precursors. All replacement reactions are endothermic.

Solvent	Solvent Displacement Energy (kJ/mol)
Pyridine	26.17
Piperidine	37.98
3,4-Lutidine	33.34

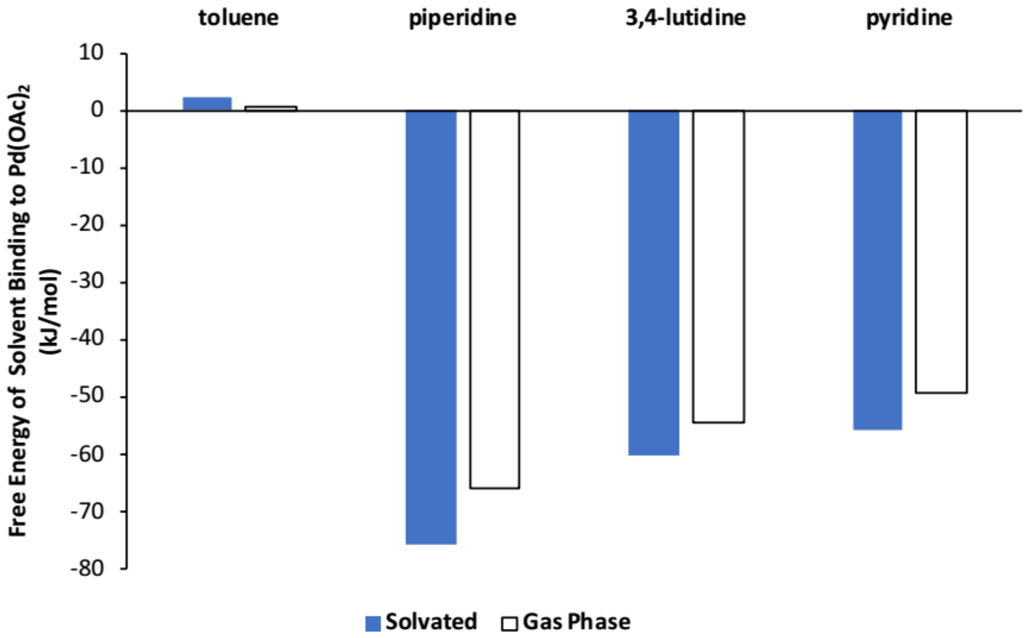

Figure S17 Gibbs free energy of $Pd(OAc)_2$ + solv→ $Pd(OAc)_2(solv)$ in the gas phase (First Step in Figure 3), and solvated phase with a COSMO implicit solvent with the dielectric constant of the pure solvent phase present.

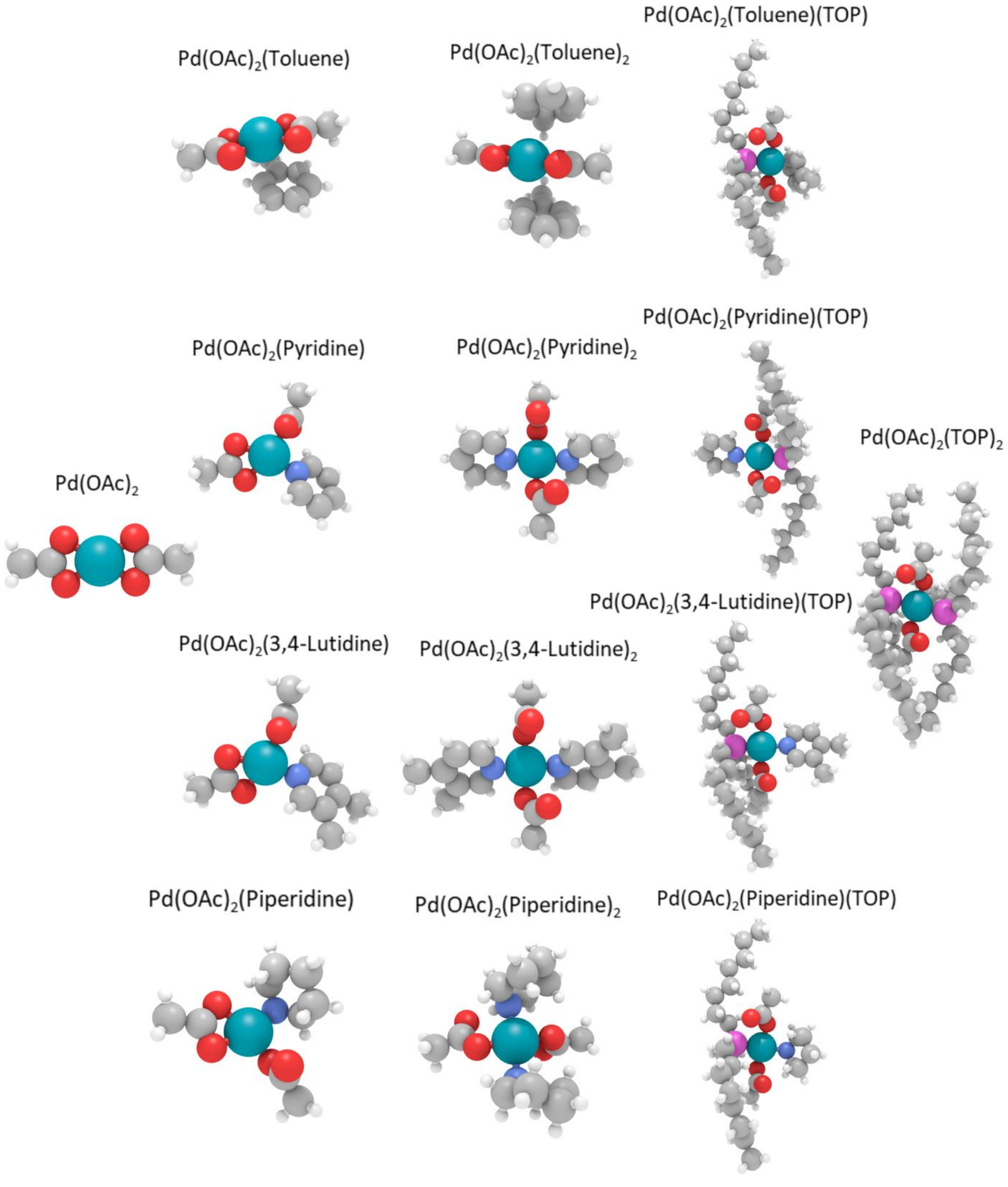

$Pd(OAc)_2(Toluene)$

$Pd(OAc)_2(Toluene)_2$

$Pd(OAc)_2(Toluene)(TOP)$

$Pd(OAc)_2$

$Pd(OAc)_2(Pyridine)$

$Pd(OAc)_2(Pyridine)_2$

$Pd(OAc)_2(Pyridine)(TOP)$

$Pd(OAc)_2(TOP)_2$

$Pd(OAc)_2(3,4\text{-}Lutidine)$

$Pd(OAc)_2(3,4\text{-}Lutidine)_2$

$Pd(OAc)_2(3,4\text{-}Lutidine)(TOP)$

$Pd(OAc)_2(Piperidine)$

$Pd(OAc)_2(Piperidine)_2$

$Pd(OAc)_2(Piperidine)(TOP)$

Figure S18 Rendered images of all precursors shown in Figure 3. Color code of atoms: Pd – teal, N - light blue, H - white, O - red, P- magenta, and C - gray.

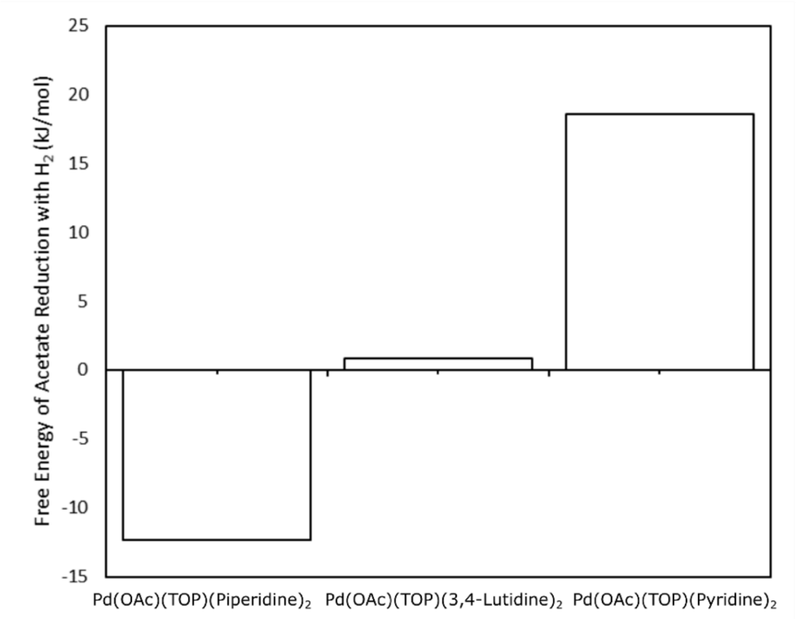

Figure S19 Gibbs free energy of H_2 reduction of Pd(OAc)(TOP)(solv)$_2$ precursors from DFT calculations.

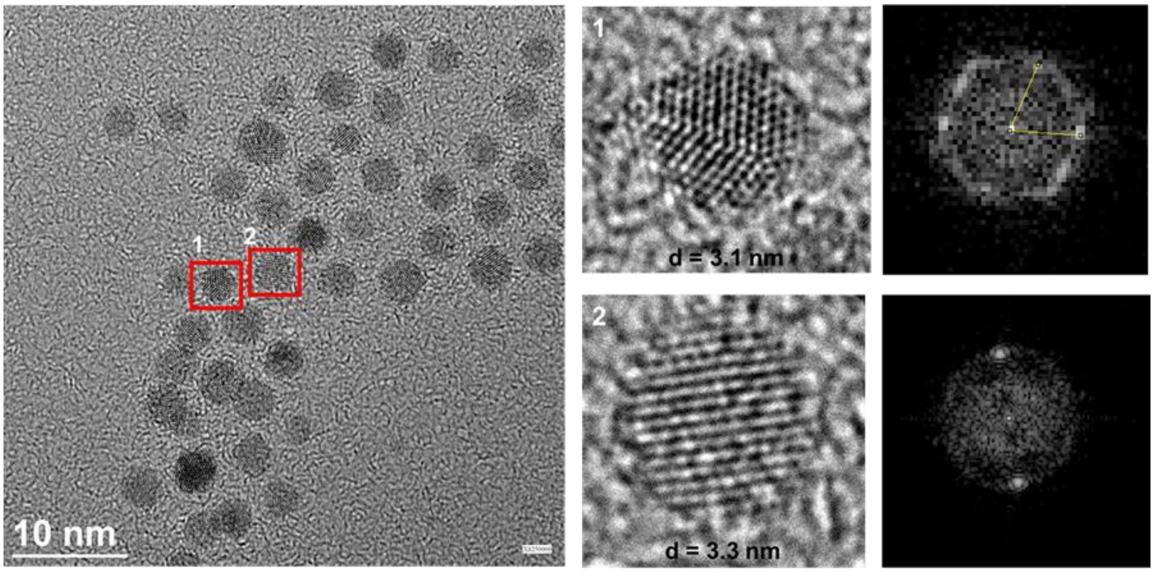

Figure S20 A representative TEM image at time = 1 hr for the Pd colloidal nanoparticles synthesized in pyridine/hexanol. Particle 1 (3.1 nm) and 2 (3.3 nm) were selected to show the FFT analysis for the crystal structure. The d-spacing results are both 0.23 nm, which is consistent with the d-spacing of the Pd(111) surface. Pd(OAc)2 = 10 mM, TOP = 20 mM, temperature = 100 °C.

In the TEM images, most of the nanoparticles were single crystalline, but polycrystalline nanoparticles were also observed. Polycrystallinity has been often observed in colloidal metal nanoparticles[13], which was believed to be caused by different factors, such as oxidative etching[14, 15] and growth by agglomeration. However, the increase in the number of nanoparticles during the reaction indicates that the growth via agglomeration is not the main mechanism for the growth of Pd nanoparticles studied herein, as agglomeration often causes a significant drop in the number of nanoparticles followed by fast increase in the average nanoparticle size[16, 17]. We also note that many nanoparticles were disordered, which is commonly seen when strong capping ligands bind to the surface such as phosphine, sulfur and sulfate ligands[18-21]. Therefore, we attribute the disorder and polycrystallinity to the strong binding of TOP to the surface causing strain and possibly leading to preferential growth on some particles.

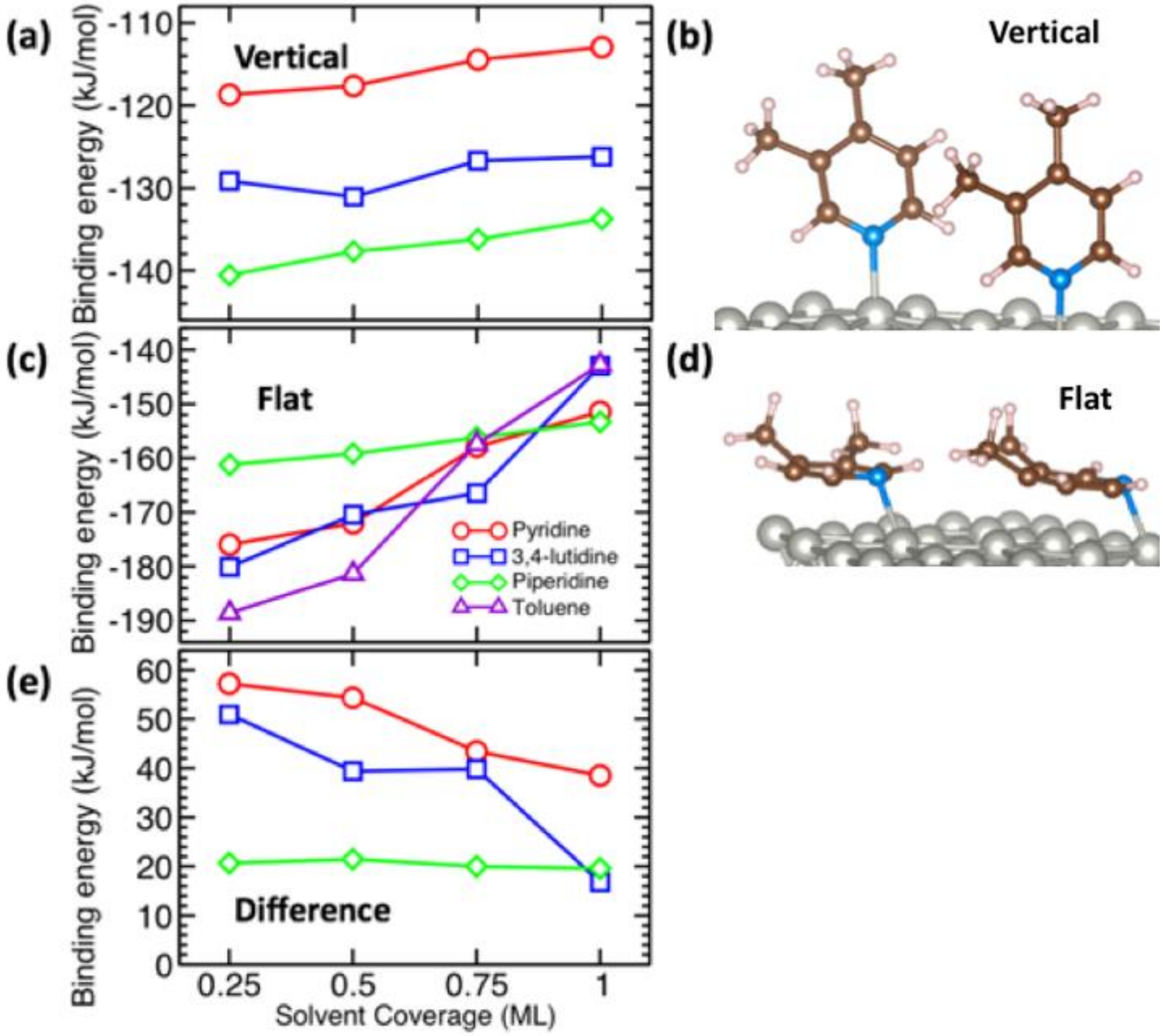

Figure S21 Binding energy (BE) per mole of solvent with coverage ranging from 0.25 monolayer (ML) to 1 ML with solvents bound (a,b) vertically and (c,d) flat. (e) The difference between vertical and flat binding for solvents allowing both configurations, except toluene which only binds flat.

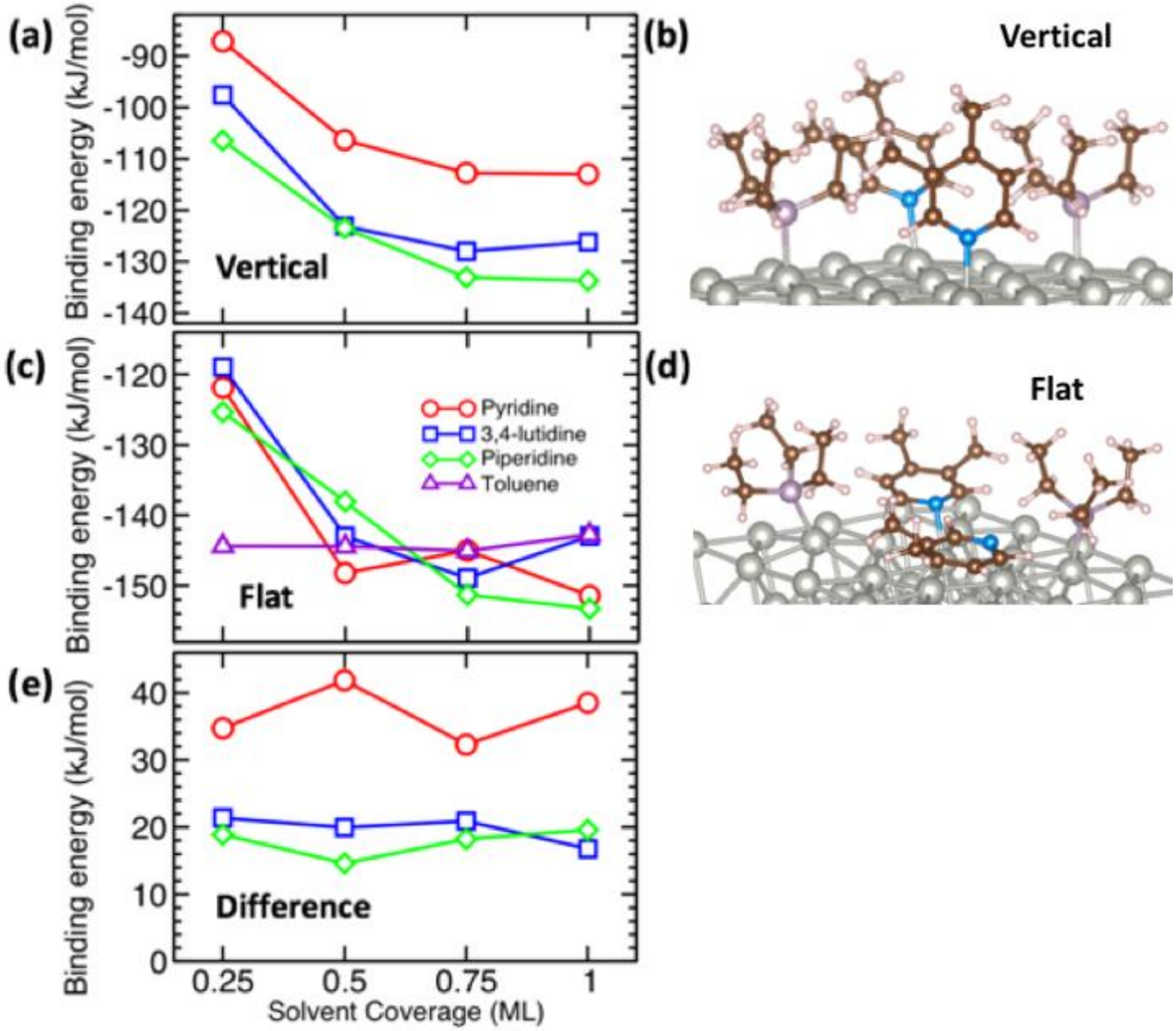

Figure S22 Binding energy (BE) per mole of solvent with coverage ranging from 0.25 monolayer (ML) to 1 ML with solvents bound (a,b) vertically and (c,d) flat. TEP occupies remaining sites on the Pd (111) surface. (e) The difference between vertical and flat binding for solvents allowing both configurations, except toluene which only binds flat.

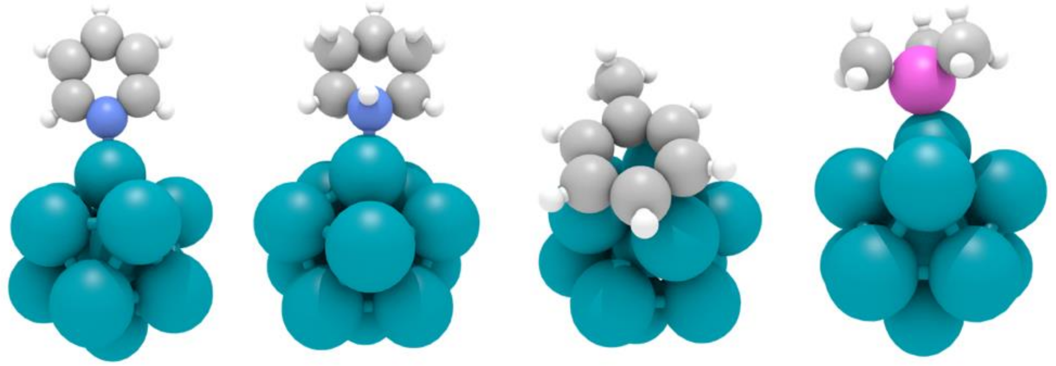

Pyridine-Pd_{13} BE=-129 kJ/mol

Piperidine-Pd_{13} BE=-171 kJ/mol

Toluene-Pd_{13} BE=-219 kJ/mol

TMP-Pd_{13} BE=-219 kJ/mol

Figure S23 DFT calculation results on binding modes and binding energies (BE) of solvents and trimethyl phosphine (TMP) on icosahedral 13 atoms Pd nanoparticle surface. Binding energies follow same trend observed for Pd (111) as shown in Figure 6. Color code of atoms: Pd – teal, N - light blue, H - white, O - red, P – magenta, and C – gray.

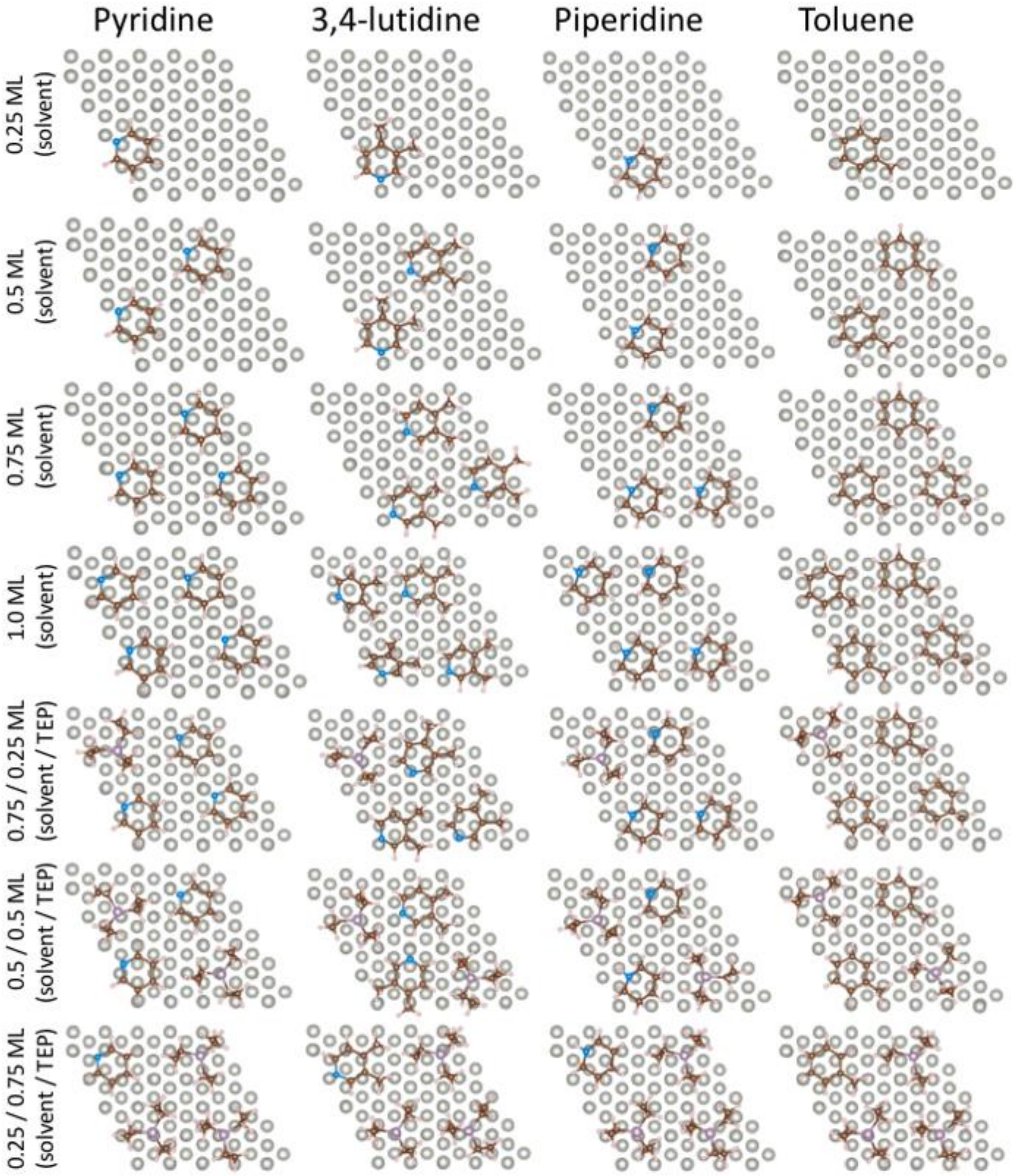

Figure S24 DFT optimized geometries of flat binding modes of solvents with and without triethylphosphine (TEP) on Pd (111) surface. Nitrogen atoms are shown in blue and phosphorous atoms are shown in light purple.

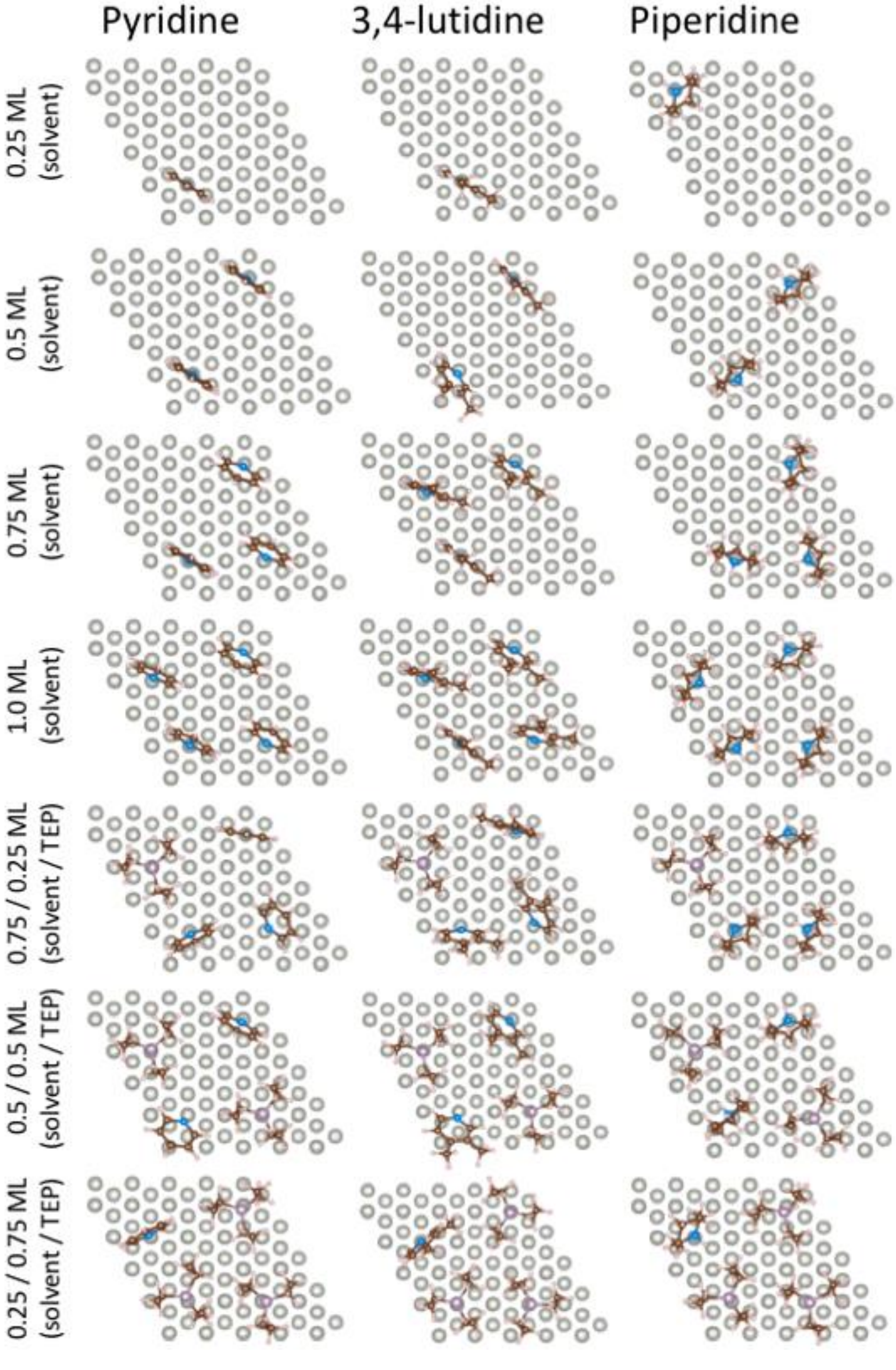

Figure S25 DFT optimized geometries of vertical binding modes of solvents with and without triethylphosphine (TEP) on Pd (111) surface. Toluene only binds flat and is therefore not included. Nitrogen atoms are shown in blue and phosphorous atoms are shown in light purple.

References

1. S. Mozaffari, W. Li, C. Thompson, S. Ivanov, S. Seifert, B. Lee, L. Kovarik and A. M. Karim, *Nanoscale*, 2017, **9**, 13772-13785.
2. X. Chen, J. Schröder, S. Hauschild, S. Rosenfeldt, M. Dulle and S. Förster, *Langmuir*, 2015, **31**, 11678-11691.
3. K. Adachi and H. Watarai, *Journal of Materials Chemistry*, 2005, **15**, 4701-4710.
4. S. Mozaffari, W. Li, C. Thompson, S. Ivanov, S. Seifert, B. Lee, L. Kovarik and A. M. Karim, *Nanoscale*, 2017, **9**, 13772-13785.
5. K. An and G. A. Somorjai, *ChemCatChem*, 2012, **4**, 1512-1524.
6. M. Harada and Y. Kamigaito, *Langmuir*, 2012, **28**, 2415-2428.
7. S. R. K. Perala and S. Kumar, *Langmuir.*, 2014, **30**, 12703-12711.
8. S. R. K. Perala and S. Kumar, *Langmuir*, 2013, **29**, 9863-9873.
9. B. Abécassis, F. Testard, Q. Kong, B. Francois and O. Spalla, *Langmuir*, 2010, **26**, 13847-13854.
10. K. Cao, J. Biskupek, C. T. Stoppiello, R. L. McSweeney, T. W. Chamberlain, Z. Liu, K. Suenaga, S. T. Skowron, E. Besley, A. N. Khlobystov and U. Kaiser, *Nature Chemistry*, 2020, **12**, 921-928.
11. A. M. Karim, N. Al Hasan, S. Ivanov, S. Siefert, R. T. Kelly, N. G. Hallfors, A. Benavidez, L. Kovarik, A. Jenkins, R. E. Winans and A. K. Datye, *J. Phys. Chem. C*, 2015, **119**, 13257-13267.
12. S. Mozaffari, W. Li, C. Thompson, S. Ivanov, S. Seifert, B. Lee, L. Kovarik and A. M. Karim, *Journal of visualized experiments: JoVE*, 2018.
13. L. Polavarapu, S. Mourdikoudis, I. Pastoriza-Santos and J. Pérez-Juste, *CrystEngComm*, 2015, **17**, 3727-3762.
14. C. M. Cobley, M. Rycenga, F. Zhou, Z.-Y. Li and Y. Xia, *Angew. Chem. Int. Ed.*, 2009, **48**, 4824-4827.
15. J. Zhang, C. Feng, Y. Deng, L. Liu, Y. Wu, B. Shen, C. Zhong and W. Hu, *Chem. Mater.*, 2014, **26**, 1213-1218.
16. M. Harada and R. Ikegami, *Crystal Growth & Design*, 2016, **16**, 2860-2873.
17. J. Polte, T. T. Ahner, F. Delissen, S. Sokolov, F. Emmerling, A. F. Thünemann and R. Kraehnert, *J. Am. Chem. Soc.*, 2010, **132**, 1296-1301.
18. H. You and J. Fang, *Nano Today*, 2016, **11**, 145-167.
19. B. Gilbert, F. Huang, Z. Lin, C. Goodell, H. Zhang and J. F. Banfield, *Nano Lett.*, 2006, **6**, 605-610.
20. G. Corthey, J. A. Olmos-Asar, G. Casillas, M. M. Mariscal, S. Mejía-Rosales, J. C. Azcárate, E. Larios, M. José-Yacamán, R. C. Salvarezza and M. H. Fonticelli, *J. Phys. Chem. C*, 2014, **118**, 24641-24647.
21. Y. Liu, C. Wang, Y. Wei, L. Zhu, D. Li, J. S. Jiang, N. M. Markovic, V. R. Stamenkovic and S. Sun, *Nano Lett.*, 2011, **11**, 1614-1617.